This supplement provides more detailed information about the moisture source diagnostics

The Lagrangian moisture source diagnostics applied in this study was developed by Sodemann et al. (2008) for identifying the moisture sources of precipitation. Here it is adapted to explain the total sub-cloud layer humidity in Barbados similarly as in Pfahl and Wernli (2008). With this technique, evaporation sites of the moisture can be identified by following the air parcels back in time and registering changes in specific humidity along the trajectories (Fig. S1.1).

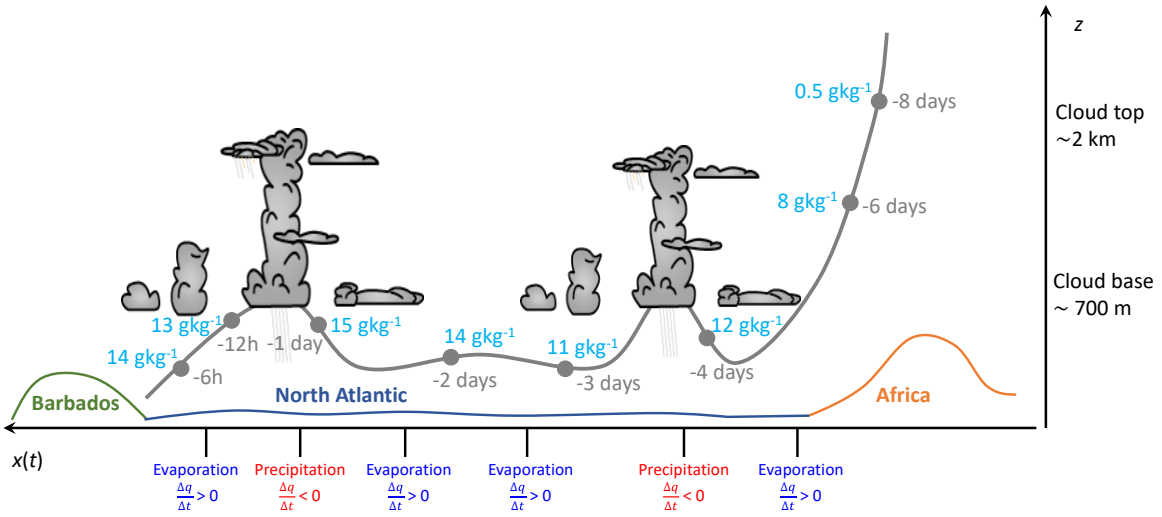

Figure S1.1: Schematic of the evolution of specific humidity along an air parcel (grey line) descending from the extratropical mid troposphere in front of the North African coast and traversing the North Atlantic following a typical trade wind pathway. The specific humidity of the air parcel is indicated in light blue at a few selected time steps. Evaporation events are indicated in blue along the x-axis and precipitation events in red. In our setup with ERA5 trajectories we consider hourly values along the trajectory (Δt=1h). This figure is inspired by Sodemann et al. (2008) and Läderach and Sodemann (2016).

The water budget for diagnosing changes of the specific humidity q in a Eulerian framework can be written as

$$\frac{\partial}{\partial t}(q\rho) + \nabla(q\rho\boldsymbol{u}) = Q, \qquad (1)$$

where t is the time, ρ the density of air, $\boldsymbol{u}$ the wind velocity, and Q a source and sink term. Assuming mass continuity, we have $q\left(\frac{\partial \rho}{\partial t} + \nabla(\rho\boldsymbol{u})\right) = 0$ and thus:

$$\rho\frac{\partial q}{\partial t} + \rho\boldsymbol{u}\nabla q = Q. \qquad (2)$$

Changes of specific humidity along a trajectory

$$\frac{Dq}{Dt} = \frac{\partial q}{\partial t} + \boldsymbol{u}\nabla q \quad (3)$$

can only occur due to the term Q in Eq. (2) associated with sub-grid scale processes such as surface evaporation from the ocean or the land surface, turbulent mixing in or above the boundary layer, shallow or deep convection, and microphysical processes involving phase changes of water. Furthermore, numerical errors can impact the budget due to trajectory position errors e.g. at locations

with strong gradients and interpolation of *q* to the trajectory position. In the method of Sodemann et al. (2008), changes in *Q* are assumed to primarily occur due to surface evaporation or precipitation thus simplifying the overall budget to one source and one sink of water vapour of an air parcel.

Positive hourly increments in specific humidity along trajectories are regarded as moisture uptakes from the underlying surface at the center of the corresponding trajectory segment (Fig. S1.2). Each uptake location is weighted according to its contribution to the final humidity of a trajectory arriving in the sub-cloud layer. If a decrease in specific humidity (i.e., precipitation) occurs along a trajectory after one or more uptakes, the weights of the previous uptakes are discounted (see Sodemann et al., 2008, for a detailed description).

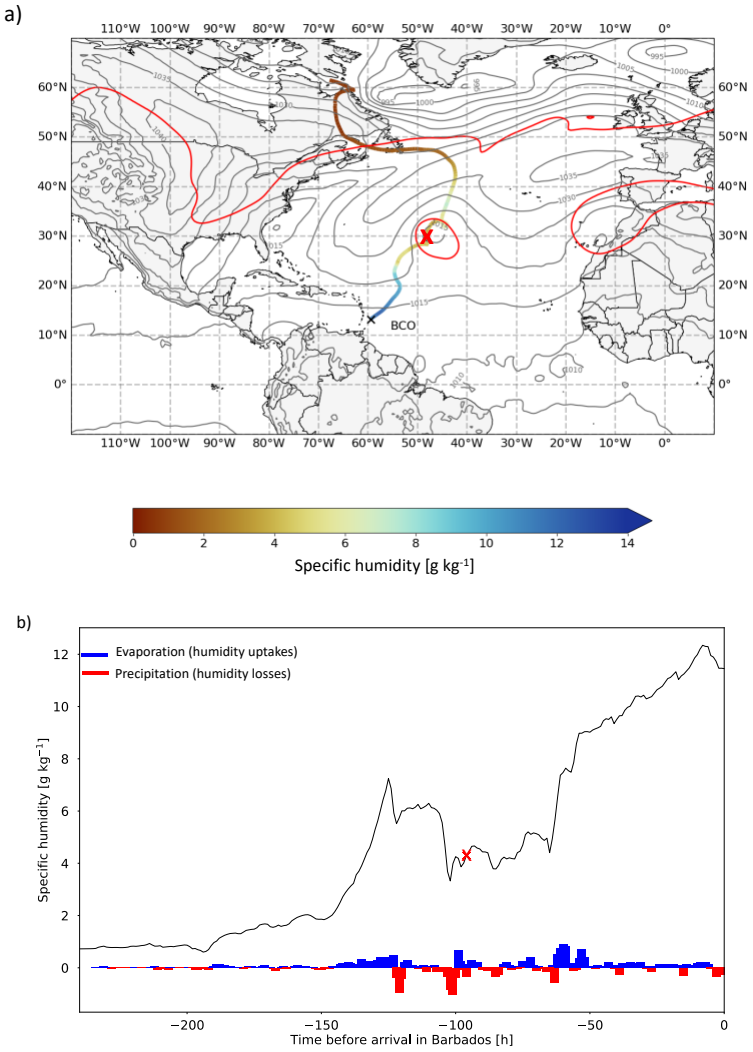

Figure S1.2: Humidity uptake and loss along an exemplary dry intrusion trajectory arriving in Barbados at 15 UTC on 2 February 2018. (a) shows this trajectory colored with specific humidity. The red cross marks the position 4 days before arrival in Barbados. The red line shows the 2-pvu contour on 320 K, grey lines mark sea level pressure contours 4 days before arrival. (b) Time evolution of *q* along the trajectory, with uptake and loss events marked in blue and red, respectively. Note that *t=0* on the right of the diagram corresponds to the arrival time of the trajectory in Barbados.

For a given time step, the moisture source contribution of the different trajectories is weighted according to their final specific humidity (i.e. their contribution to the sub-cloud layer humidity at the measurement site). The moisture uptakes from the trajectories are then gridded for each hourly time step onto a regular 1° horizontal grid. Composite fields of moisture sources for each flow regime are obtained by weighting the moisture source fields by the mean sub-cloud layer specific humidity at the arrival point and integrating over all time steps associated with the respective flow regime. For two example time steps we show the trajectories (Fig. S1.3) and the specific humidity evolution along them (Fig. S1.4). The resulting gridded moisture sources are shown in Fig. S1.5.

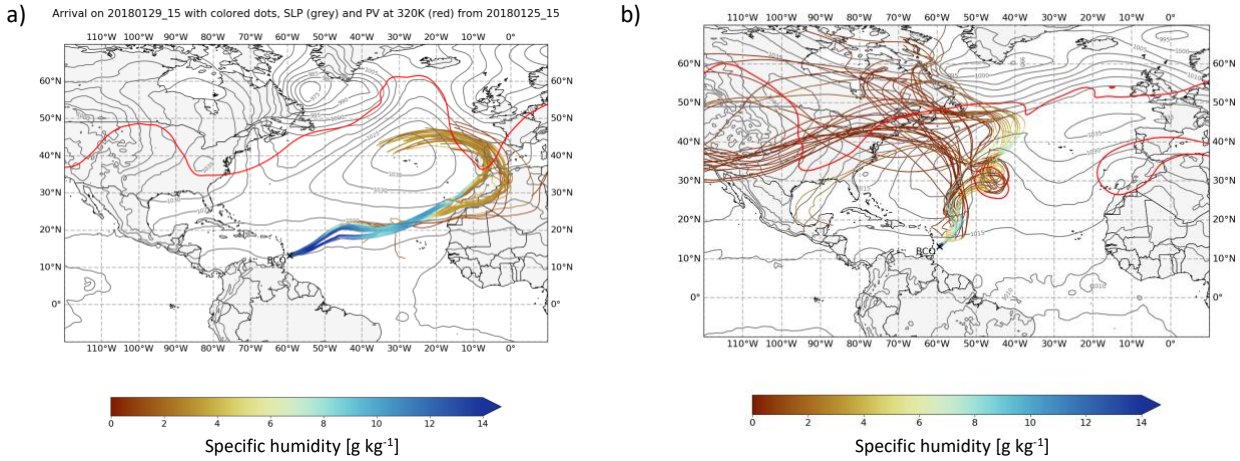

Figure S1.3: Specific humidity (in colors) along the trajectories arriving in the sub-cloud layer at 15 UTC on 29 January 2018 (a, extratropical trade wind case) and 15 UTC on 2 February 2018 (b, extratropical dry intrusion case).

The specific humidity evolution along the exemplary extratropical trade wind and dry intrusion trajectories nicely illustrates the different timing of strong humidity uptake, which occurs when the air parcels dive into the boundary layer (Fig. S1.4). For the trade wind case in Fig. S1.4a, this occurs 5-6 days before arrival, while for the extratropical dry intrusion many air parcels experience rapid moistening only 2-3 days before arrival. In the manuscript this is discussed based on the weighted mean distance to the moisture source, which we compute based on the moisture source diagnostics output.

Overall for the isoTrades campaign we find that 98% of the specific humidity at arrival is explained by the applied algorithm. This is a very high explained fraction, compared to other studies, in which we have used high resolution data from the regional numerical weather prediction model COSMO (7-14 km) for computing the trajectories and where we typically found lower values of explained moisture fraction (~80%, e.g. Aemisegger et al., 2014; Suess et al., 2019; Thurnherr et al. 2020) due to trajectories moving out of the model domain.

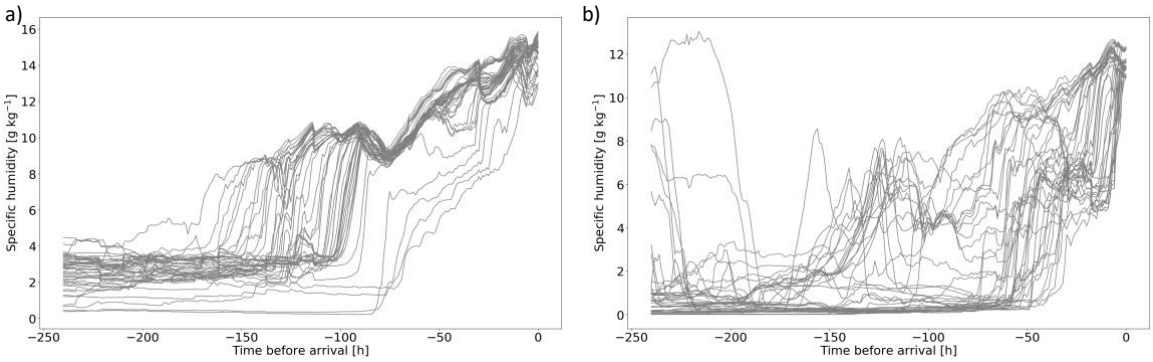

Figure S1.4: Time evolution of the specific humidity along all the 40 trajectories arriving in the sub-cloud layer at 15 UTC on 29 January 2018 (a, extratropical trade wind case) and 15 UTC on 2 February 2018 (b, extratropical dry intrusion case).

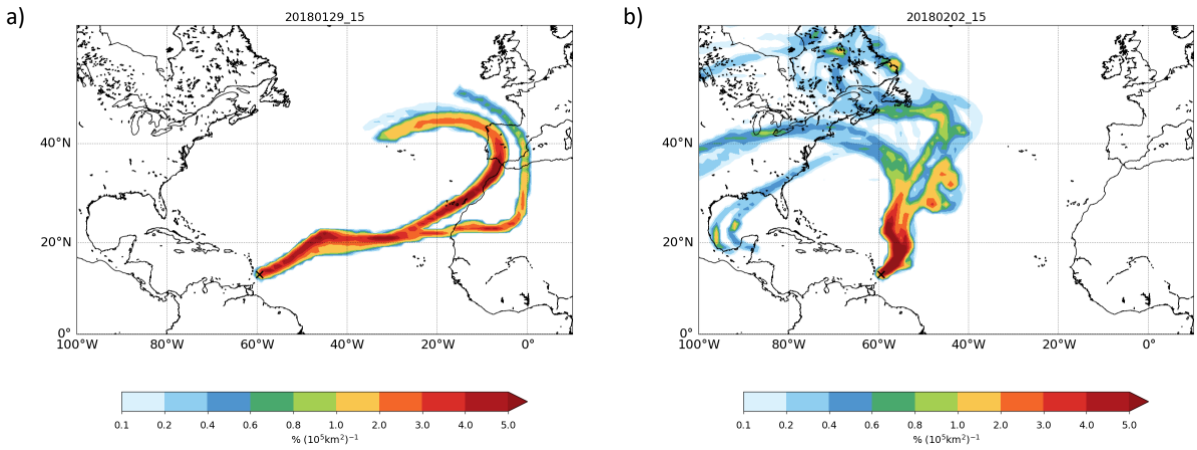

Figure S1.5: Moisture source distribution diagnosed from trajectories arriving in the sub-cloud layer at 15 UTC on 29 January 2018 (a, extratropical trade wind case) and 15 UTC on 2 February 2018 (b, extratropical dry intrusion case).

An important parameter in the moisture source diagnostic is the maximum altitude, at which an uptake is assumed to be vertically linked to surface evaporation. Here we consider all uptakes (within the boundary layer and above) to be influenced by surface evaporation. We find that for isoTrades 86% of all moisture uptakes occur in the boundary layer and 14% above the boundary layer[1]. Detailed inspection of individual trajectories shows that in the trade wind region, air parcels can experience uptakes with a clear vertical link with surface evaporation, due to shallow convection, even though occurring well above the diagnosed model boundary layer. In these cases, the vertical link with surface evaporation is due to convective mixing of boundary layer air upward in the atmospheric column. Thus, no use of a maximum uptake height is applied here.

To estimate the relevance of uptakes due to cloud and below cloud evaporation, we applied the above method introducing an attribution procedure of uptakes depending on environmental conditions

[1] Note, that in ERA5, the boundary layer top is diagnosed based on the Richardson number and is usually located at the altitude of cloud base and not at the trade inversion (see von Engeln and Teixeira, 2013).

along the trajectories (similarly as done by Dütsch et al. (2018) for mixing processes). We assume that an increase in specific humidity along a trajectory is due to cloud or below cloud evaporation, if the specific hydrometeor content at the trajectory segment mid-point is larger than 0.05 g kg^{-1}. With this approach, we find that in total 6% of the uptakes occur in the presence of hydrometeors, 5% in the boundary layer, and 1% above. Furthermore, when distinguishing between falling hydrometeors (snowflakes and rain droplets) and in-cloud hydrometeors (cloud liquid water and ice), we observe that a large majority of the uptakes are due to cloud evaporation (99.2% of all hydrometeor-related uptakes). We therefore conclude, that when using the setup of this study, the simplifying assumption that a large majority of the humidity uptakes along the trajectories are associated with surface evaporation, is adequate.

References

Aemisegger, F., Pfahl, S., Sodemann, H., Lehner, I., Seneviratne, S. I., and Wernli, H.: Deuterium excess as a proxy for continental moisture recycling and plant transpiration, Atmos. Chem. Phys., 14, 4029–4054, https://doi.org/10.5194/acp-14-4029-2014, 2014.

Dütsch, M., Pfahl, S., Meyer, M., and Wernli, H.: Lagrangian process attribution of isotopic variations in near-surface water vapour in a 30-year regional climate simulation over Europe, Atmos. Chem. Phys., 18, 1653–1669, https://doi.org/10.5194/acp-18-1653-2018, 2018.

von Engeln, A. and Teixeira, J.: A planetary boundary layer height climatology derived from ECMWF reanalysis data, J. Climate, 26, https://doi.org/6575-6590, 10.1175/JCLI-D-12-00385.1, 2013.

Läderach, A., and Sodemann, H.: A revised picture of the atmospheric moisture residence time, Geophys. Res. Lett., 43, 924–933, https://doi.org/10.1002/2015GL067449, 2016.

Pfahl S. and Wernli H.: Air parcel trajectory analysis of stable isotopes in water vapor in the eastern Mediterranean, J. Geophys. Res.-Atmos., 113, D20104, https://doi.org/10.1029/2008JD009839, 2008.

Sodemann, H., Schwierz, C., and Wernli, H.: Interannual variability of Greenland winter precipitation sources: Lagrangian moisture diagnostic and North Atlantic Oscillation influence, J. Geophys. Res.-Atmos., 113, D03107, https://doi.org/10.1029/2007JD008503, 2008.

Suess, E., Aemisegger, F., Sonke, J., Sprenger, M., Wernli, H., and Winkel, L.: Marine versus continental sources of iodine and selenium in rainfall at two European high-altitude locations, Environ. Sci. and Technol., 19:53,1905-1917, https://doi.org/10.1021/acs.est.8b05533, 2019.

Thurnherr, I., Hartmuth, K., Jansing, L., Gehring, J., Boettcher, M., Gorodetskaya, I., Werner, M., Wernli, H., and Aemisegger, F.: The role of air–sea fluxes for the water vapour isotope signals in the cold and warm sectors of extratropical cyclones over the Southern Ocean, Weather Clim. Dynam. Discuss., https://doi.org/10.5194/wcd-2020-46, revised, 2020.